Title

An implantable multifunctional neural microprobe for simultaneous multi-analyte sensing and chemical delivery

Journal

Lab on a Chip, 20(8)

ISSN

1473-0197

Authors

Wang, Bo
Wen, Ximiao
Cao, Yan
et al.

Publication Date

2020-04-21

DOI

10.1039/d0lc00021c

Peer reviewed

HHS Public Access

Author manuscript

Lab Chip. Author manuscript; available in PMC 2021 April 21.

Published in final edited form as:

Lab Chip. 2020 April 21; 20(8): 1390–1397. doi:10.1039/d0lc00021c.

An Implantable Multifunctional Neural Microprobe for Simultaneous Multi-Analyte Sensing and Chemical Delivery

Bo Wang[1,5,†], **Ximiao Wen**[†,2], **Yan Cao**[3], **Shan Huang**[4], **Hoa Lam**[1], **Tingyi "Leo" Liu**[6], **Pei-Shan Chung**[7], **Harold G. Monbouquette**[3], **Pei-Yu Chiou**[2,7,*], **Nigel T. Maidment**[1,*]

[1]Department of Psychiatry & Biobehavioral Sciences, Semel Institute for Neuroscience and Human Behavior, University of California at Los Angeles, California, USA

[2]Department of Mechanical and Aerospace Engineering, University of California at Los Angeles, California, USA

[3]Department of Chemical and Biomolecular Engineering, University of California at Los Angeles, California, USA

[4]Department of Biological Chemistry, University of California at Los Angeles, California, USA

[5]Department of Electrical and Computer Engineering, University of California at Los Angeles, California, USA

[6]Department of Mechanical and Industrial Engineering, University of Massachusetts Amherst, Massachusetts, USA

[7]Department of Bioengineering, University of California at Los Angeles, CA, USA

Abstract

A multifunctional chemical neural probe fabrication process exploiting PDMS thin-film transfer to incorporate a microfluidic channel onto a silicon-based microelectrode array (MEA) platform, and enzyme microstamping to provide multi-analyte detection is described. The Si/PDMS hybrid chemtrode, modified with a nano-based on-probe IrOx reference electrode, was validated in brain phantoms and in rat brain.

Graphical abstract

[*]Corresponding authors at: University of California, Los Angeles, CA 90095, USA Nigel T. Maidment (nmaidmen@g.ucla.edu), Pei-Yu Chiou (pychiou@seas.ucla.edu).

† These authors contributed equally to this work

Author contributions

B. W. and X. W. designed and manufactured the probes, conducted the *in vitro* and *in vivo* characterizations, analyzed the data and produced initial drafts of the manuscript. X. W. and T. L. developed the PDMS thin-film transfer process. Y. C. assisted in the enzyme microstamping procedure. S. H. and H. L. provided surgical expertise. P.-S. C. assisted in the impedance measurement. H. G. M., P. -Y. C. and N. T. M. conceived and supervised the project and contributed to the writing and editing of the manuscript.

Conflicts of interest

There are no conflicts to declare.

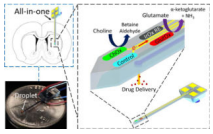

PDMS thin-film transfer and enzyme microstamping enabled 3-in-1 Si/PDMS hybrid chemtrode for multi-analyte sensing and chemical Delivery *in vivo*

Implantable neural microprobes are widely used in neuroscience studies for chemical and electrophysiological recordings of neural activities in deep brain regions.[1–5] The probes are often used in conjunction with local chemical delivery systems to manipulate neural circuits. Conventionally, in order to achieve simultaneous electrochemical recording of multiple analytes (*e.g.*, dopamine, glutamate, and acetylcholine), which work together to control complex behaviors, and chemical modulation, multiple implants are required, including (1) multiple electrochemical sensors for different analytes; (2) counter electrode (CE) and reference electrode (RE), or RE also acting as CE; and (3) an independent microinjector separated from or glued manually onto the shank of the sensing electrodes[6–8] for chemical delivery (Figure 1a, left). Such an approach requires prolonged surgical implantation procedures and results in significant damage to the brain. Moreover, the relative distance between separated chemical delivery devices, sensing electrodes, and RE can be hard to control, hampering experimental reproducibility and introducing variability in baseline noise[9]. Therefore, the development of a multifunctional probe that integrates these individual components into a single implantable device is highly desirable (Figure 1a, right).

To this end, advances in MEMS technology have been harnessed to create silicon microelectrode array (MEA) microprobes with integrated microfluidic channels on the same shank using bulk or surface micromachining[10]. Compared to conventional approaches such as gluing glass pipettes to the probes, sophisticated microfluidic functions such as multi-channel delivery and on-probe mixing can be achieved with minimal increase in probe dimension[11, 12]. In bulk micromachining, the channel is formed by etching the silicon substrate, which is sealed by either depositing materials isotropically, such as by plasma enhanced chemical vapor deposition (PECVD) of silicon dioxide[13, 14], or by wafer bonding[11, 15]. In surface micromachining, the channel is formed by removal of sacrificial film deposited on top of the silicon substrate[16, 17]. Such silicon-based chemtrodes are batch fabricated with high precision; however, the process for fabricating the microfluidic channels requires multiple additional MEMS fabrication steps such as wafer bonding, polishing, film deposition and etching, which is often complicated, costly and may not be readily accessible.

Here, we describe the development of a customized PDMS thin-film transfer process based on soft lithography that enables integration of microfluidic channels on silicon microprobes. In this highly flexible process, free-standing ultra-thin PDMS microfluidic channels can be fabricated in batch mode[5, 18] with minimal increase in dimensions, or can be used to modify pre-fabricated MEAs since PDMS channels are transferred as the last step of the process. It is very convenient and cost-effective for building prototypes to iterate microfluidic channel design or to validate other functionalities on the probe (biosensing in this work) without

designing and fabricating a new batch of MEAs each time. Second, we incorporated a platinum (Pt) nanoparticle-modified IrOx reference electrode, replacing the conventional unstable Ag/AgCl film, by electrodeposition on the microprobe as previously described[3, 5, 9]. Finally, we adapted our recently developed PDMS microstamping technique[19, 20] to selectively transfer glutamate and choline oxidases onto individual electrodes of the MEA, thereby demonstrating the potential for manipulation and detection of multiple non-electroactive analytes, in this case of glutamate and of choline, a metabolite of acetylcholine, with a single implantable device. This results in a 3-in-1 multifunctional neural probe that integrates multi-analyte sensing, on-probe reference electrode and local chemical delivery.

Results and Discussion

The fabrication procedure was optimized to be compatible with our existing silicon-based neural probe design (150 μm thick, 144 μm width, and 9 mm long)[3, 21]. Here, for proof of concept, a chemtrode is demonstrated (Figure 1b-e) incorporating a Pt microelectrode array (2 × 2) at the tip, which consists of a nano-based IrOx reference electrode, a glutamate sensing electrode, a choline sensing electrode, a control electrode, and a back-sided microfluidic channel. The fabrication process (Figure 2a) is described in the Supplementary Information in detail and can be summarized as (1) integration of an ultra-thin, free-standing microfluidic channel *via* a customized PDMS thin-film transfer process (Figure 2a i-ii), (2) construction of a nano-based IrOx reference microelectrode *via* electrodeposition (Figure 2a iii-v); (3) deposition of enzyme mixture onto two closely juxtaposed permselective membrane-modified working electrodes for the detection of glutamate and choline *via* PDMS microstamping (Figure 2a vi, Supplementary Figures S1-S4).

In our thin-film transfer process, it is important to keep the top surface of the mold flat. To this end, we fabricated the mold from a polished flat top silicon wafer. Through two steps of time-controlled DRIE etching, a silicon mold with two different depths is formed to enable the transfer of free-standing ultra-thin PDMS channels in one step (Figure 2b). Specifically, one layer of PDMS thin-film with channel, cured against the silicon mold with two different depths, was transferred directly to the back side of the probe SiO_2 surface by oxygen plasma bonding to form an enclosed channel, with the silicon probe itself as the channel bottom surface and PDMS as the cover. To avoid probe fracture during the transfer process, silicon probes were temporarily fixed on a glass slide with photoresist (PR, AZ 5214/non-exposed SU-8), which was subsequently dissolved in acetone. Thanks to the rigid glass backing used to pick up the PDMS, the features are dimensionally stable. An alignment accuracy of < 5 μm can be achieved using a contact mask aligner (Neutronix Quintel 7000). This produced a PDMS microfluidic channel, with a length of 9 mm, a total thickness of 15 μm, and a channel dimension of 10 × 20 μm (thickness × width) that enables precise chemical delivery at flow rates ranging from 0.25 to 1.75 μL/min with pumping pressure from 5 to 20 psi. The tested flow rates are similar to other chemtrodes[10]. While higher flow rates could be achieved by increasing the pumping pressure up to 60 psi without PDMS delamination, such high rates increase the risk of tissue deformation and liquid backflow along the probe shank. A 40 μm-diameter fluid outlet (Figure 2c), formed in the same molding process, was placed on top of the PDMS membrane such that fluid is ejected perpendicular to the probe surface

instead of towards the probe tip to avoid channel occlusion[22] during the probe insertion process. Local injection of chemical solution (Figure 2d) with nanoliter precision can be controlled by the pumping pressure and duration. Flow rates were measured in triplicate at 4 different pumping pressures (5–20 psi) to demonstrate the expected linear relationship between pressure and flow rate ($R^2 = 0.996$) and low variability across replicate measures (Figure 2e).

In this proof of concept design, the microfluidic channel is integrated onto the back side of the existing Si probe. The ejected chemicals diffuse from the fluid outlet to the sensors on the front, separated by the thickness of the probe (150 μm). The advantage of this approach is that the sensors are less impacted by dilution effects than they would otherwise be if the fluid outlet was on the front of the probe. Nevertheless, the current setup may not be suitable for certain applications where a more localized delivery in the immediate vicinity of the electrodes is desired. In such cases, fluidic outlets can be easily fabricated on the front by either (1) transferring PDMS channels to the probe front after allocating sufficient space for the fluidic interface; or (2) creating vias in the probe shank to connect the fluidic channels on the back. Further, more sophisticated PDMS structures, with multi-channels or multi-shanks, can be molded and transferred to the corresponding Si probes in one step[5, 18]. Our prior work has demonstrated that PDMS channels with a spacing of 20 μm can be achieved providing stable, leak-free operation at 60 psi[23], such that it should be possible to accommodate 3 microfluidic channels on the current platform. In addition, the thickness of the probe can be further reduced simply by starting with a thinner silicon substrate without changing the fabrication process - silicon probes with 50 μm thickness have been fabricated in our lab. We do not anticipate problems with probe fracture during the transfer process since the probes are temporarily fixed to a glass substrate using photoresist. Further, we do not expect the long-term stability of the probes to be impacted by addition of the ultra-thin (15 μm) PDMS channel due to its extremely low stiffness (1 MPa *vs.* 100 GPa, PDMS *vs.* Si).

To construct an on-probe reference electrode, one microelectrode of the MEA was first deposited with Pt nanoparticles (PtNP) to enhance the surface area using a previously described non-cytotoxic electrodeposition procedure[3, 24, 25], followed by IrOx electrodeposition (0.0 – 0.6 V, 100 cycles). A typical cyclic voltammogram of IrOx electrodeposition on a PtNP/Pt microelectrode is shown in Supplementary Figure. S6). The IrOx film has been shown to be mechanically stable and biocompatible[26–29]. Although the potential of IrOx film shows strong pH dependence, the small dynamic range of normal brain pH (7.15–7.4) makes this issue unimportant in most cases[30]. Recently, we[9] and others[30–32] validated that the open circuit potential of the IrOx film remained stable over a two-week period. Although electrophysiological recording and electrical stimulation with IrOx electrode were not performed in this study, the impedance of the nano-based IrOx electrodes, 4.48 ± 0.25 kΩ (n = 5) at 1 kHz, was found to be significantly lower than unmodified Pt microelectrodes (~20 kΩ at 1 kHz)[5]. After the deposition of the Nafion layer, the impedance of the IrOx electrode increased to 15.21 ± 1.18 kΩ (n = 5) at 1 kHz. Here, the performance of the IrOx, as a reference electrode (RE), was verified by amperometric detection of H_2O_2, which is the byproduct of the oxidase-based enzymatic reactions, at Pt microelectrodes (0.6 V *vs.* IrOx), employing H_2O_2 concentration step changes (0 – 80 μM;

Sensitivity: 2516.1 ± 20.1 μA•mM^{-1}•cm^{-2}; Limit of Detection: 0.13 ± 0.01 μM), showing high stability and repeatability (Figure 3a). The nano-based IrOx RE was further tested in the context of glucose sensors, where crosslinked enzyme layers were applied on top of permselective membrane (poly-m-phenylenediamine (PPD) and Nafion)-modified Pt electrodes (See Supplementary Materials for details of permselective layer and enzyme deposition). The deposited PPD and Nafion layers acted as size and charge exclusion membranes, allowing hydrogen peroxide molecules to pass through to the Pt electrode surface but excluding common interferents (*e.g.*, negatively-charged ascorbic acid (AA) and positively-charged dopamine (DA)) present in the brain extracellular fluid.[18, 20, 33] The performance of a representative glucose sensor in stirred phosphate-buffered saline (PBS) solution is shown in Figure 3b showing a linear concentration-response from 0–360 uM glucose and response time of ~2 s. Further data from multiple probes is provided in Supplementary Figure S5 demonstrating a sensitivity of 52.2 ± 5.5 μA•mM^{-1}•cm^{-2} and a calculated detection limit of 1.5 ± 0.8 μM (n = 6). Selectivity is demonstrated by the lack of response to the physiological interferents, AA and DA, at physiologically relevant concentrations[34, 35] (Figure 3c).

To achieve simultaneous sensing of more than one non-electroactive analyte, PDMS stamping[11, 12] was adapted to selectively and sequentially transfer each of the two different enzyme/BSA mixtures - glutamate oxidase/BSA and choline oxidase/BSA - onto two distinct, juxtaposed microelectrodes (~100 μm separation, Figure 3d) previously coated with permselective layers as described in Supplementary Materials, followed by crosslinking via glutaraldehyde vapor (see Supplementary Materials for full details of the stamping procedure and Figures S1-S4). For dual sensing, one of the 4 microelectrodes remained free of enzyme and served as a control electrode, and another (top left) was converted to an on-probe reference electrode as described above. A schematic of the various permselective and enzyme layers of the constructed dual sensor and the sensing mechanism is shown in Figure 3e. The choline and glutamate sensors were first characterized in stirred PBS solution, separately (*i.e.* on probes with only one of the two enzymes applied, see Supplementary Materials for methods). Figure 3f and 3g show linear responses of representative electrodes to serial additions of choline and glutamate, respectively, each with a response time of ~2 s. Sensitivities for choline and glutamate of 74.8 ± 4 μA•mM^{-1}•cm^{-2} (n = 4) and 84.7 ± 15 μA•mM^{-1}•cm^{-2} (n = 3), were obtained with calculated detection limits of 4.1 ± 1.4 μM and 3.8 ± 1.9 μM, respectively (Supplementary Figure S5). Subsequently, the performance of the dual sensor platform was assessed and shown to display zero crosstalk among glutamate, choline and control sites at the concentrations tested, and to exclude interfering species (Figure 3h).

The integrated functions of electrochemical sensing and chemical delivery were initially tested in brain phantoms (0.6% w/v agarose in artificial cerebrospinal fluid, aCSF). Figure 4a shows the reproducibility of glucose detection following repeated local injection of a glucose solution (800 μM in aCSF) at 20 psi for pumping durations of 2 s and 0.2 s. Selectivity of glutamate and choline detection by the dual sensor is shown in Figure 4b. (See Supplementary Materials for further methodological details).

Validation of the integrated microbiosensor/chemical delivery platform *in vivo* was conducted with microprobes acutely inserted into the dorsal striatum of the rat brain. Figure 4c shows glucose detection following repeated local injection of 4 mM glucose at 20 psi with increasing injection durations. The more transient nature of the signals compared to injections into brain phantoms is likely due to active uptake of glucose. Interestingly, the amplitude of the signal reached a plateau at an injection duration of 1.2 s, but the area under the curve continued to increase. This may be due to acute activation of glucose transport, a possibility supported by the overshooting below baseline after injection, but this requires further investigation. Preliminary validation of the glutamate/choline dual sensor is shown in Figure 4d demonstrating detection of both glutamate and choline following injections of a mixture of the two compounds. The need for higher concentrations of analytes when delivered to live brain tissue compared to static agar phantoms is likely due to the presence of both active cellular uptake mechanisms and diffusion into circulating blood in the former condition, reducing the concentration attained at the electrode surface. We observed the same phenomenon in our previous studies[5]. Post-calibration of the sensors upon removal from the brain demonstrated a less than 20% reduction in signal amplitude for the three analytes, compared with pre-calibration data. Such decreases are commonly reported for all types of implantable electrochemical sensors and is attributed to biofouling (*e.g.*, protein aggregation on the sensor surface). The shelf life of the fabricated sensors is limited by the stability of both the on-probe IrOx reference electrode and enzymes on the electrode surfaces. For the IrOx reference electrode, we[9] previously demonstrated that the performance was stable for at least 2 weeks and preferred to use them within a day or two of their preparation. Similarly, we have not tested the probes beyond two weeks *in vivo*. The long-term stability and biocompatibility of the sensors will be a subject for future investigation and may include incorporation of anti-fouling biopolymers such as 2-methacryloyloxethylphosporylcholine (MPC)[36–38].

Conclusion

We present an approach to the fabrication of multi-functional neural microprobes using a novel PDMS thin-film transfer process to transfer microfluidic channels to silicon-based neural probes. Incorporation of PDMS enzyme stamping and an integrated on-probe reference electrode permits simultaneous detection of multiple analytes together with local delivery of agents that can both validate biosensor function and manipulate neuronal activity. Although a single microfluidic channel was employed here, the approach can be readily scaled up with additional channels for multiple chemical delivery. The integration of these multiple functions on a single platform removes the need for implanting multiple probes, with the dual benefits of reducing brain damage and surgical complexity.

Supplementary Material

Refer to Web version on PubMed Central for supplementary material.

Acknowledgement

This work was supported by NIH grant R01NS087494. All microfabrication steps were completed using equipment provided by the UCLA Nanoelectronics Research Facility.

References

1. Obidin N, Tasnim F. and Dagdeviren C, Adv. Mater, 2019, 1901482.
2. Seymour JP, Wu F, Wise KD and Yoon E, Microsystems & Nanoengineering, 2017, 3, 16066. [PubMed: 31057845]
3. Wang B, Feng L, Koo B. and Monbouquette HG, Electroanal., 2019, 31, 1249–1253.
4. Wassum K, Tolosa V, Wang J, Walker E, Monbouquette H. and Maidment N, Sensors, 2008, 8, 5023–5036. [PubMed: 19543440]
5. Wen XM, Wang B, Huang S, Liu TY, Lee MS, Chung PS, Chow YT, Huang IW, Monbouquette HG, Maidment NT and Chiou PY, Biosens. Bioelectron, 2019, 131, 37–45. [PubMed: 30818131]
6. Zhou J, Zhang L. and Tian Y, Anal. Chem, 2016, 88, 2113–2118. [PubMed: 26768309]
7. Frey O, Holtzman T, McNamara R, Theobald D, Van Der Wal P, De Rooij N, Dalley J. and Koudelka-Hep M, Sensors and Actuators B: Chemical, 2011, 154, 96–105.
8. Walker E, Wang J, Hamdi N, Monbouquette HG and Maidment NT, Analyst, 2007, 132, 1107–1111. [PubMed: 17955144]
9. Tolosa VM, Wassum KM, Maidment NT and Monbouquette HG, Biosens. Bioelectron, 2013, 42, 256–260. [PubMed: 23208095]
10. Sim JY, Haney MP, Park SI, McCall JG and Jeong J-W, Lab Chip, 2017, 17, 1406–1435. [PubMed: 28349140]
11. Shin H, Lee HJ, Chae U, Kim H, Kim J, Choi N, Woo J, Cho Y, Lee CJ and Yoon E-S, Lab Chip, 2015, 15, 3730–3737. [PubMed: 26235309]
12. Lee HJ, Son Y, Kim J, Lee CJ, Yoon E-S and Cho I-J, Lab Chip, 2015, 15, 1590–1597. [PubMed: 25651943]
13. Chen J, Wise KD, Hetke JF and Bledsoe SC, IEEE. T. Bio-med. Eng, 1997, 44, 760–769.
14. Retterer ST, Smith KL, Bjornsson CS, Neeves KB, Spence AJ, Turner JN, Shain W. and Isaacson MS, IEEE. T. Bio-med. Eng, 2004, 51, 2063–2073.
15. Seidl K, Spieth S, Herwik S, Steigert J, Zengerle R, Paul O. and Ruther P, J. Micromech. Microeng, 2010, 20, 105006.
16. Lin L. and Pisano AP, J. Microelectromech. S, 1999, 8, 78–84.
17. Neeves K, Lo C, Foley C, Saltzman W. and Olbricht W, J. Control Release, 2006, 111, 252–262. [PubMed: 16476500]
18. Liu TL, Wen X, Kung Y-C and Chiou PY, 2017 IEEE 30th International Conference on Micro Electro Mechanical Systems (MEMS), 663–666.
19. Wang B, Koo B, Huang LW and Monbouquette HG, Analyst, 2018, 143, 5008–5013. [PubMed: 30226501]
20. Wang B, Koo B. and Monbouquette HG, Electroanal., 2017, 29, 2300–2306.
21. Tseng TTC and Monbouquette HG, J. Electroanal. Chem, 2012, 682, 141–146.
22. Chen Z-J, Gillies GT, Broaddus WC, Prabhu SS, Fillmore H, Mitchell RM, Corwin FD and Fatouros PP, J. Neurosurg, 2004, 101, 314–322. [PubMed: 15309925]
23. Kung Y-C, Huang K-W, Fan Y-J and Chiou P-Y, Lab Chip, 2015, 15, 1861–1868. [PubMed: 25710255]
24. Boehler C, Stieglitz T. and Asplund M, Biomaterials, 2015, 67, 346–353. [PubMed: 26232883]
25. Wang B, Wen X, Chiou PY and Maidment NT, Electroanal., 2019, 31, 1641–1645.
26. Yamanaka K, Jpn. J. Appl. Phys, 1989, 28, 632–637.
27. Weiland JD and Anderson DJ, IEEE. T. Bio-med. Eng, 2000, 47, 911–918.
28. Slavcheva E, Vitushinsky R, Mokwa W. and Schnakenberg U, J. Electrochem. Soc, 2004, 151, E226–E237.
29. Marzouk SA, Ufer S, Buck RP, Johnson TA, Dunlap LA and Cascio WE, Anal. Chem, 1998, 70, 5054–5061. [PubMed: 9852787]
30. Franklin RK, Johnson MD, Scottt K, Shim JH, Nam H, Kipket D. and Brown RB, IEEE Sensors Journal, 2005, 1400–1403.

31. Franklin RK, Joo S, Negi S, Solzbacher F. and Brown RB, IEEE Sensors Journal, 2009, 1086–1089.
32. Yang H, Kang SK, Choi CA, Kim H, Shin D-H, Kim YS and Kim YT, Lab Chip, 2004, 4, 42–46. [PubMed: 15007439]
33. Wahono N, Qin S, Oomen P, Cremers T, de Vries M. and Westerink B, Biosensors and Bioelectronics, 2012, 33, 260–266. [PubMed: 22326702]
34. Eriksson E, Engberg G, Bing O. and Nissbrandt H, Neuropsychopharmacol, 1999, 20, 287–296.
35. Spector R, N Engl J Med, 1977, 296, 1393–1398. [PubMed: 323714]
36. Ye SH, Watanabe J, Iwasaki Y. and Ishihara K, Biomaterials, 2003, 24, 4143–4152. [PubMed: 12853244]
37. Goda T, Tabata M, Sanjoh M, Uchimura M, Iwasaki Y. and Miyahara Y, Chem. Commun, 2013, 49, 8683–8685.
38. Sibarani J, Takai M. and Ishihara K, Colloids and Surfaces B: Biointerfaces, 2007, 54, 88–93. [PubMed: 17112710]

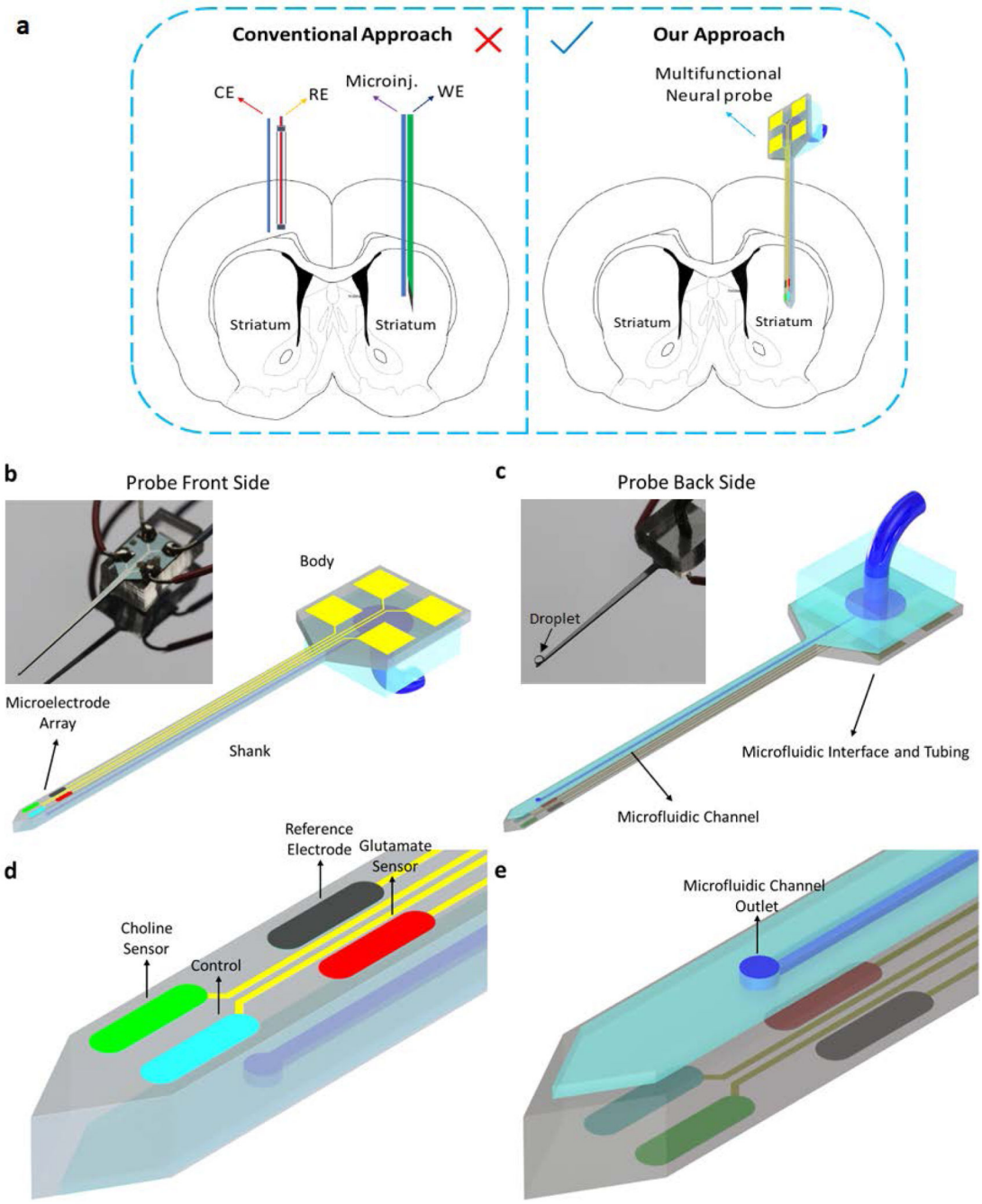

Figure 1.

(a) Schematic diagram showing conventional chemical sensing and agent delivery system *vs.* our single multifunctional neural probe. (b-e) Conceptual diagram of the proposed multi-functional neural probe with chemical delivery and multi-sensing capabilities. (b) Front side of the microprobe; (c) Back side of the microprobe; (d) Chemtrode shank tip (front side) showing the functionalized microelectrode array; (e) Microprobe shank tip (back side) showing the outlet of the microfluidic channel.

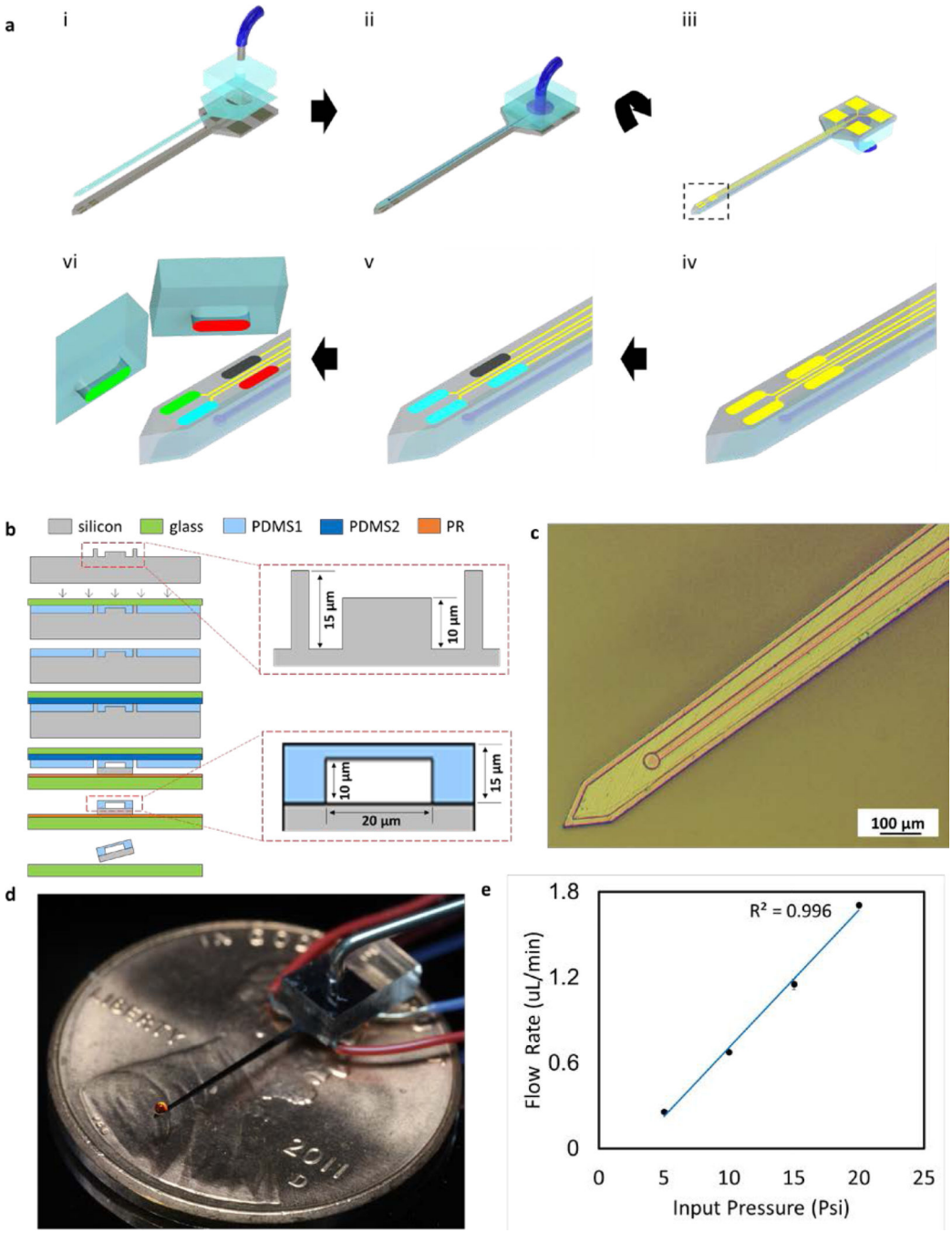

Figure 2.

a) Multi-functional neural probe fabrication process. i) An exploded-view drawing of the microfluidic channel on the back of the microprobe; ii) Back side of the microprobe; iii) Front side of the microprobe; iv) Microprobe shank tip showing Pt microelectrode array (Yellow); v) Reference electrode (Black) and permselective membrane coating (Light Blue); vi) PDMS stamping to transfer two different enzymes to designated microelectrodes (Red and Green). b) Customized thin-film transfer process for microfluidic channel fabrication. c) Optical image showing the outlet of the microfluidic channel at the back of the probe tip. d)

Optical image showing the delivery of dye solution to the outlet of the microfluidic channel at the back of the probe tip. e) Demonstration of a linear relationship between flow rate and pumping pressure ($R^2 = 0.996$) and high repeatability of the measure (n = 3 per pressure point for a representative microprobe). Error bar: standard error.

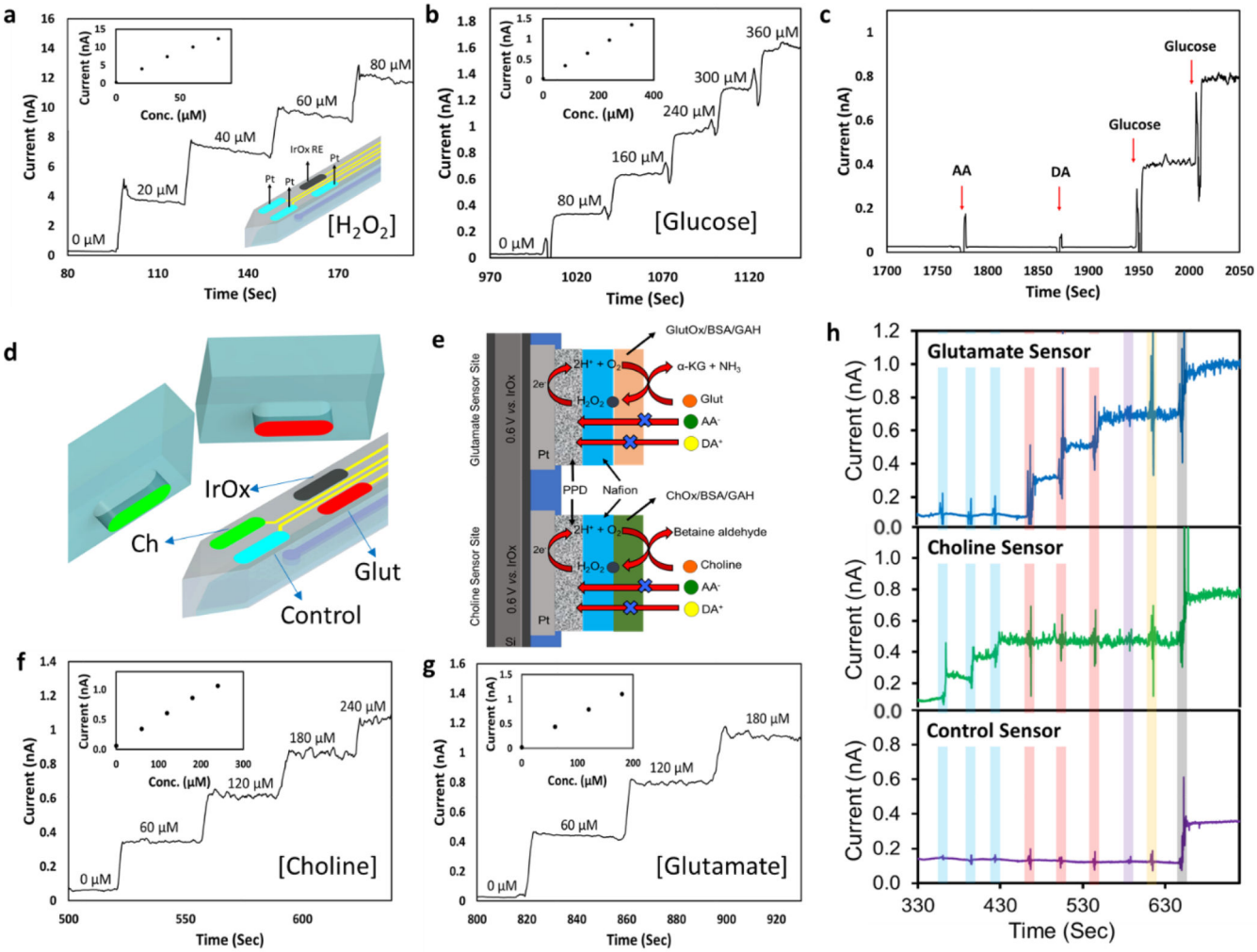

Figure 3.

a) A representative current-time response of the microelectrode array to increasing concentrations of H_2O_2 with IrOx as an on-probe reference electrode (0.6 V *vs.* IrOx). Insert: plot of current *vs.* H_2O_2 concentration. b) A representative current-time response of the microelectrode array to increasing concentrations of glucose with IrOx as an on-probe reference electrode (0.6 V *vs.* IrOx). Insert: plot of current *vs.* glucose concentration. c) A representative current-time response to glucose and electroactive interferents. The sensor response at a constant potential of 0.6 V (*vs.* IrOx) was monitored upon sequential injections to give 250 μM AA, 5 μM DA, 160 μM glucose, and 320 μM glucose. d) Schematics of a microelectrode array showing the location of the IrOx reference electrode, control electrode, and enzyme stamped glutamate and choline sensors. e) Schematic of the final dual glutamate/choline sensor configuration. f) A representative current-time response of a choline oxidase-stamped electrode (of an MEA limited to such coated electrodes) to increasing concentrations of choline (0.6 V *vs.* IrOx). Insert: plot of current *vs.* choline concentration. g) A representative current-time response of a glutamate oxidase-stamped electrode (of an MEA limited to such coated electrodes) to increasing concentrations of glutamate (0.6 V *vs.* IrOx). Insert: plot of current *vs.* glutamate concentration. h) Combined

sensing of glutamate and choline on a representative MEA at a constant potential of 0.6 V (*vs.* Ag/AgCl). The individual sensor responses of the MEA were monitored upon sequential injections to give stepwise final concentrations as follows: 60 μM choline, 120 μM choline,180 μM choline (blue), 180 μM choline/60 μM glutamate, 180 μM choline/120 μM glutamate, 180 μM choline/180 μM glutamate (pink), 180 μM choline/180 μM glutamate/250 μM AA (purple), 180 μM choline/180 μM glutamate/250 μM AA/5 μM DA (yellow), and 180 μM choline/180 μM glutamate/250 μM AA/5 μM DA/20 μM H_2O_2 (grey).

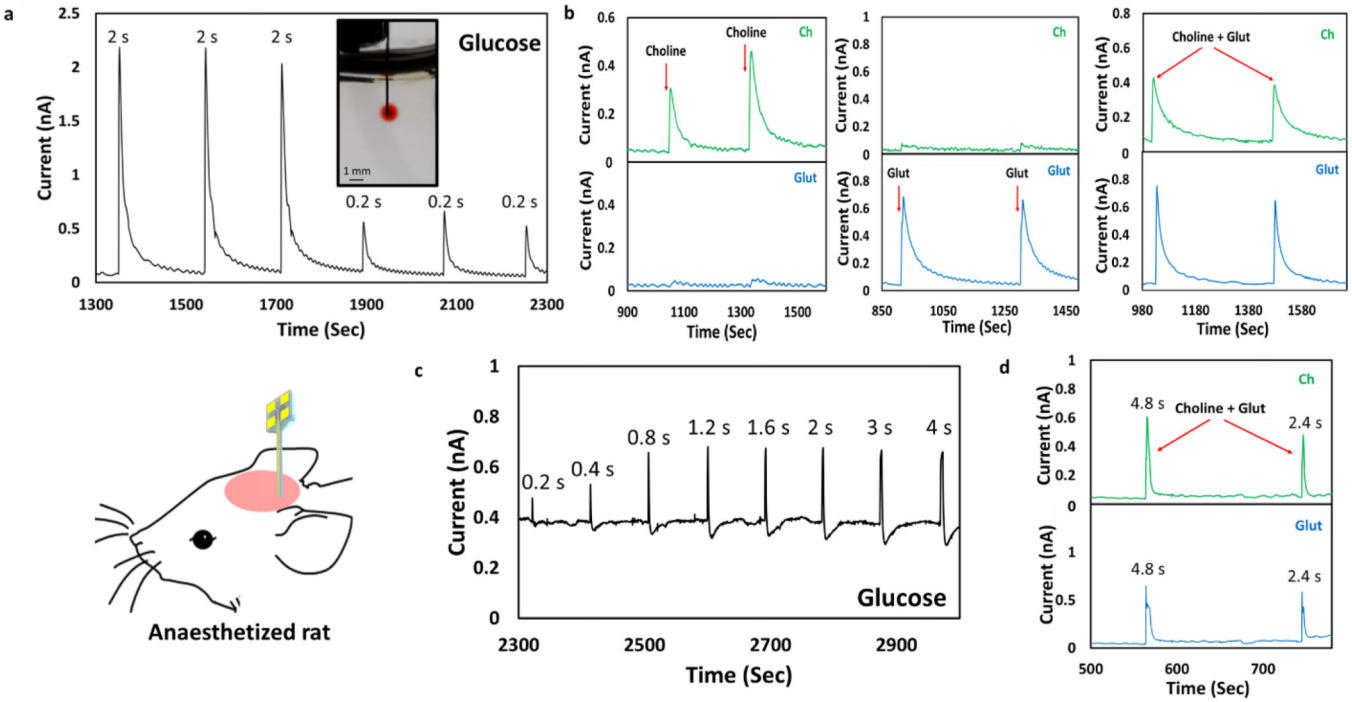

Figure 4.

Sensor validation in brain phantoms and *in vivo*. a) *In vitro* testing of 800 μM glucose injection and detection in 0.6% agarose gel. The slow decrease in the glucose concentration is due to pure diffusion in this un-mixed medium. Pumping pressure: 20 psi. Insert: Optical image demonstrating delivery of liquid (aqueous solution with red dye) into a brain phantom (0.6% agarose gel). b) Selectivity of glutamate (Glut) and choline (Ch) dual sensor. From left to right: local injection of choline or glutamate alone (800 μM in aCSF) and a choline/glutamate mixture (800 μM in aCSF). Pumping pressure: 10 psi. c) *In vivo* glucose (4 mM) injection and sensing in rat striatum. Injection pressure was kept at 20 psi with increasing injection duration. d) Dual detection of glutamate and choline in rat striatum following injection of a choline/glutamate mixture in aCSF (50 mM for each analyte). Pumping pressure 20 psi.